

LASER INTERFEROMETER GRAVITATIONAL WAVE OBSERVATORY  
- LIGO -  
CALIFORNIA INSTITUTE OF TECHNOLOGY  
MASSACHUSETTS INSTITUTE OF TECHNOLOGY

Technical Note	LIGO-T1400511-v1	2014/11/01
<b>An Optical Setup for Crackle Noise Detection</b>		
Carell Hamil, Gabriele Vajente, Eric Quintero		

*Distribution of this document:*  
LIGO Scientific Collaboration

**Draft**

**California Institute of Technology**  
**LIGO Project, MS 18-34**  
**Pasadena, CA 91125**  
Phone (626) 395-2129  
Fax (626) 304-9834  
E-mail: info@ligo.caltech.edu

**Massachusetts Institute of Technology**  
**LIGO Project, Room NW17-161**  
**Cambridge, MA 02139**  
Phone (617) 253-4824  
Fax (617) 253-7014  
E-mail: info@ligo.mit.edu

**LIGO Hanford Observatory**  
**Route 10, Mile Marker 2**  
**Richland, WA 99352**  
Phone (509) 372-8106  
Fax (509) 372-8137  
E-mail: info@ligo.caltech.edu

**LIGO Livingston Observatory**  
**19100 LIGO Lane**  
**Livingston, LA 70754**  
Phone (225) 686-3100  
Fax (225) 686-7189  
E-mail: info@ligo.caltech.edu

<http://www.ligo.caltech.edu/>

# 1 Introduction

## 1.1 Mechanical Upconversion and Crackling Noise

Metals are not perfect crystals, and thus, when they are stressed, there might occur some local deformations due to grain slippage or similar microscopic events. Due to mechanical upconversion, these impulsive events will sum up and give us a broad-band noise which is called “crackling noise”. A more general definition of crackling noise comes from Sethna et al [1], who define crackling noise as an “event that arises when a system responds to changing external conditions through discrete, impulsive events spanning a broad range of sizes”. This broad concept of crackle noise is further expanded with respect to the LIGO Interferometers, by Quintero et al [2], who deem it to be anything from impulsive releases of energy to acoustic emissions or changes in the geometry of attachments between suspension elements or possibly even the stress fields that may occur in the elements themselves.

There are many instances of noise occurring in the LIGO interferometers, and significant effort has gone into the investigation and reduction of these noise instances. We are primarily concerned with the crackling noise phenomenon as it has been suspected that it might be involved in the production of excess noise in various joint interfaces and suspension components of the LIGO Interferometers [2]. More specifically, one of the possible locations of occurrences of crackling noise is the maraging steel blades which are used for vertical isolation.

The group which I have joined is concerned with the investigation of the mechanical upconversion noise in steel. Essentially, this involves measuring the amount of displacement noise which might be generated by non linear phenomenon in the maraging steel blades. The Advanced LIGO detector uses steel blades as a way to suspend the mirrors and isolate them from the seismic motion of the ground. However, if the magnitude of the noise introduced by the blades is too large, the sensitivity of the detector is limited.

## 1.2 The Crackle Experiment

While the presence of multiple instances of crackling noise at different locations has been suspected in the LIGO Interferometers, the investigation of crackling noise in maraging steel blades was chosen for the first crackle experiment as these blades present a straightforward mechanical system which can be driven and stressed easily. In Advanced LIGO, the crackling is vertical noise and the coupling to the horizontal motion of the test masses is small. Due to this constraint, the vertical noise in the maraging steel blades is directly measured in the crackle experiment, so as to have maximum sensitivity to the crackling noise. For the setup, a Michelson Interferometer which has end mirrors, has been mounted to loaded springs driven by a low frequency, common-mode force. For the Advanced LIGO Interferometers, the blade motion is filtered through two pendulum stages, thus, in the smaller scale crackle experiment, the relevant measurements are made using a Michelson Interferometer at a lower displacement sensitivity than for Advanced LIGO, since the blade displacements are being measured directly. The crackling noise will be found in the differ-

ential displacement signal of the Michelson Interferometer, since it occurs incoherently in each blade [2]. The displacement noise will be measured and the results analyzed in order to find the crackle noise. The motivation behind building an improved crackle experiment is to have a new setup with better sensitivity, and with lower limitations as compared to the initial crackle setup. An experiment with improved sensitivity will help greatly in the detection of any crackle signals, as none have been found thus far.

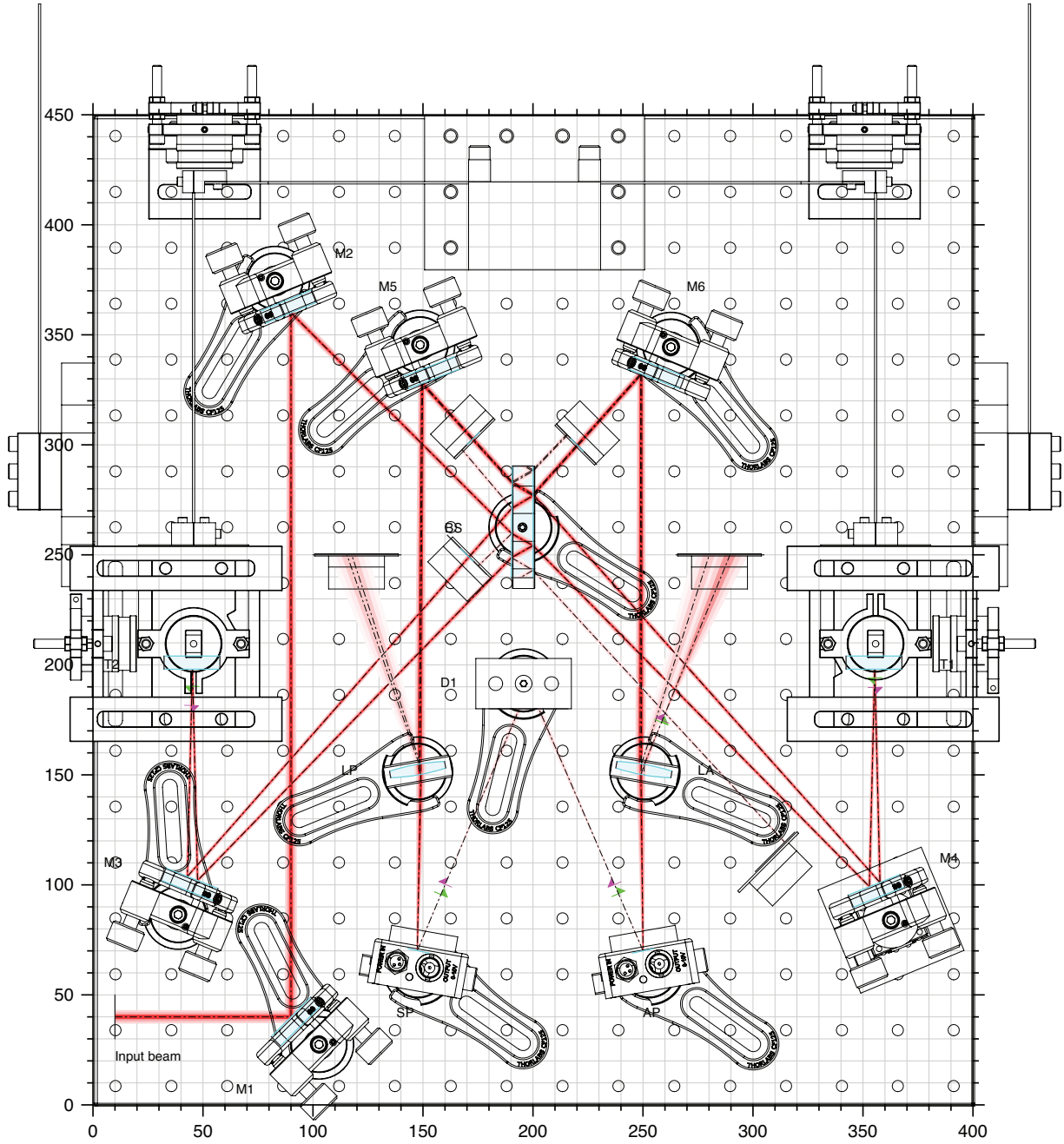
My contribution to the crackle project was the construction and alignment of the input telescope for the optical setup for the new crackle experiment. This was done according to the guidelines of the design model.

## 2 The Optical Setup

The project consisted of the construction of a the input telescope of the new, fully functional optical setup. A successful outcome for this project greatly benefited the main crackle experiment, as the correct beam size and position for the Gaussian beam needed to be fed into the optical setup. Due to the increased sensitivity of the setup, it will be determined whether or not the low frequency variations of an external stress applied to steel (which can modulate the upconversion noise level at higher frequencies) is relevant to the suspension system for the advanced gravitational wave detectors being built.

The work on this project was done in collaboration with Gabriele Vajente, Eric Quintero, and Rana Adhikari.

We can now introduce a rendering of a detailed schematic drawing of the optical setup, into which the input telescope will feed the correct Gaussian beam at a certain position, to be discussed later on in the report. Ni et al [3], proposed this configuration and design for the optical setup in their proposal for an upgraded crackle experiment, and it is shown in Fig. 1, constructed using the Optocad software, with the use Solidworks for the mechanics.



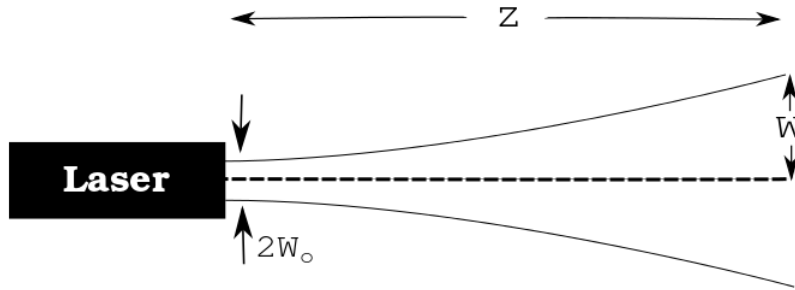
OptoCad (v 0.93k), 10 Apr 2014, crackle\_v2\_solidworks.ps

Figure 1: Detailed schematic diagram of the optical layout

### 3 Experimental Work

#### 3.1 Measuring of the Beam Parameters

For our experiment, we will be determining the beam parameters of a 1064 nm laser.



**Figure 2:** A diagram showing the parameters of a Gaussian beam.

For a Gaussian Beam propagating in the  $z$  direction, it is narrowest at  $z = 0$  or  $z = z_{waist}$ , where the Gaussian beam has a minimum value, or a “waist”,  $w_0$ , as shown in Fig. 9.

As we will be doing measurements involving the intensity distribution of the power of the laser, it will be useful to also define the radius,  $w(z)$ , of the laser, as the width at which the intensity of the Gaussian beam has decreased to  $\frac{1}{e^2}$  of its peak or axial value at various positions along the  $z$  axis. The following equation shows how the width of the beam is related to the waist,  $w_0$ , at different positions in the  $z$  axis :

$$w(z) = w_0 \left[ 1 + \left( \frac{\lambda z}{\pi w_0^2} \right)^2 \right]^{\frac{1}{2}} \quad (1)$$

As the beam spreads away from the waist, it follows a hyperbolic outline. The asymptotes of this outline give the beam divergence at far distances away from the waist, where the divergence angle at the  $\frac{1}{e^2}$  radius in the intensity distribution can be defined mathematically as :

$$\theta = \lim_{z \rightarrow \infty} \frac{w(z)}{z} = \frac{\lambda}{\pi w_0} \quad (2)$$

## 3.2 Profiling a Gaussian Beam

### 3.2.1 The Knife-Edge Measurement Method

Two methods were used to obtain measurements to aid in the computation of the Gaussian beam profile, the first being the knife-edge measurement technique. It involved measuring the total power of the beam as a razor blade was translated through the beam using a calibrated translation stage.

Initially, the total of the power of the laser beam was measured. The razor blade which was mounted on a translation stage was moved incrementally to get different values of the power over a series of distances, until the measured power was at zero. These measurements were taken at different positions along the z axis, since Gaussian beams propagate along the z axis.

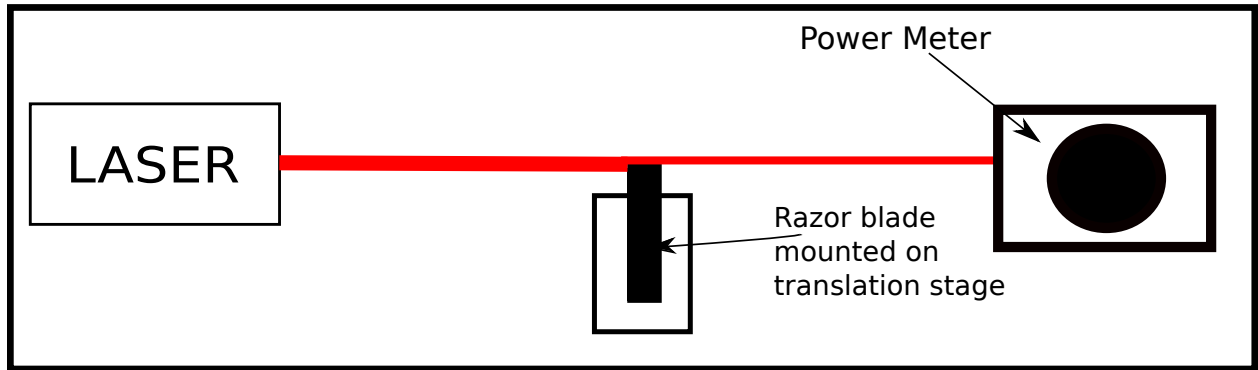


**Figure 3:** A diagram showing a simplified schematic of the setup for the knife-edge method.

The intensity distribution of a Gaussian beam is defined in the following equation:

$$I(x,y) = I_0 e^{-\frac{2x^2}{w_x^2}} e^{-\frac{2y^2}{w_y^2}} \quad (3)$$

Where  $I_0$  is the intensity at the center of the beam,  $w_x$  and  $w_y$  are the beam radii in the x and y directions respectively.

We know that the total power of the Gaussian beam is given by:

$$P = I_0 \int_{-\infty}^{+\infty} e^{-\frac{2x^2}{w_x^2}} dx \int_{-\infty}^{+\infty} e^{-\frac{2y^2}{w_y^2}} dy = \frac{\pi}{2} I_0 w_x w_y \quad (4)$$

However, for the knife-edge technique, the the razor blade was translated in the x direction, with  $P(X)$  being defined as the power measured as a function of the blade position. Hence, the equation was rearranged to the following :

$$\begin{aligned}
P(X) &= P - \int_{-\infty}^X e^{-\frac{2x^2}{w_x^2}} dx \int_{-\infty}^{+\infty} e^{-\frac{2y^2}{w_y^2}} dy \\
&= P - \sqrt{\frac{\pi}{2}} I_0 w_y \int_{-\infty}^X e^{-\frac{2x^2}{w_x^2}} dx \\
&= P - \sqrt{\frac{\pi}{2}} I_0 w_y \left[ \int_{-\infty}^0 e^{-\frac{2x^2}{w_x^2}} + \int_0^X e^{-\frac{2x^2}{w_x^2}} dx \right] \\
&= P - \sqrt{\frac{\pi}{2}} I_0 w_y \left[ \sqrt{\frac{\pi}{8}} w_x + \int_0^X e^{-\frac{2x^2}{w_x^2}} dx \right] \\
&= \frac{P}{2} - \sqrt{\frac{\pi}{2}} I_0 w_y \int_0^X e^{-\frac{2x^2}{w_x^2}} dx \tag{5}
\end{aligned}$$

In order to arrange Eq. 5 into a more standard form, the following substitution,  $s^2 = \frac{2x^2}{w_x^2}$  was made so that  $dx = \frac{w_x ds}{\sqrt{2}}$ , and then the limits of the integral were changed. This resulted in :

$$\begin{aligned}
P(X) &= \frac{P}{2} - \sqrt{\frac{\pi}{2}} I_0 w_y \int_0^{\frac{\sqrt{2}X}{w_x}} e^{-s^2} \frac{w_x}{\sqrt{2}} ds \\
&= \frac{P}{2} - \sqrt{\frac{\pi}{2}} I_0 w_y w_x \frac{2}{\sqrt{\pi}} \int_0^{\frac{\sqrt{2}X}{w_x}} e^{-s^2} ds \tag{6}
\end{aligned}$$

To arrive at the equation needed to develop the MATLAB fit function model, we will introduce the Gaussian error function :

$$erf(x) = \frac{2}{\sqrt{\pi}} \int_0^x e^{-t^2} dt \tag{7}$$

This Gaussian error function and the expression for the total power in the beam as measured in the x direction in Eq. 6, give us a final equation which we will use to construct our MATLAB model for mapping the beam profile :

$$P(X) = \frac{P}{2} \left[ 1 - erf \left( \frac{\sqrt{2}X}{w_x} \right) \right] \tag{8}$$

From this equation, a MATLAB model for mapping the beam profile was developed and this model was used to fit the experimental results to the error function of the Gaussian Beam.

The function, “fitfun”, for the error function is defined below :

$$fitfun = P(1) + \frac{P(2)}{2} \left[ 1 - erf \left( \frac{X - P(3)}{P(4)} \right) \right] \quad (9)$$

Where  $P(1)$  is the background power,  $P(2)$  is the maximum difference in power (essentially the maximum power),  $P(3)$  is the position of the beam center, and  $P(4)$  is a scaling factor related to the beam width, such that  $w = \frac{P(4)}{\sqrt{2}}$ .

Two set of measurements which were taken through the knife-edge technique are shown in Table 1 and Table 2.

The graphical results for these four sets of the measurements after they were fitted to the error function are shown in Fig. 8 below.



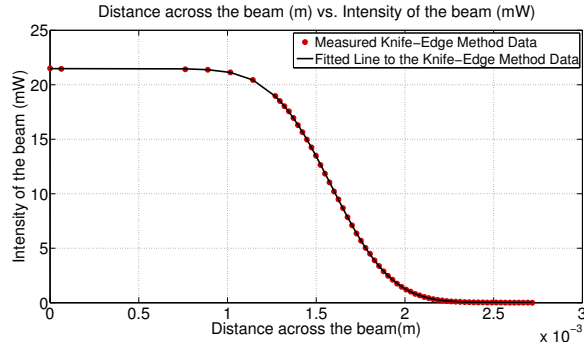


Figure 4: Measurement three

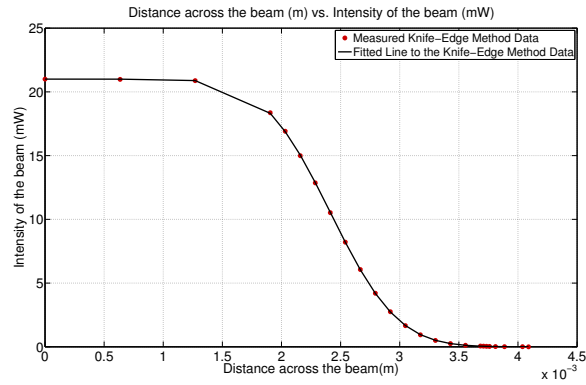


Figure 5: Measurement eight

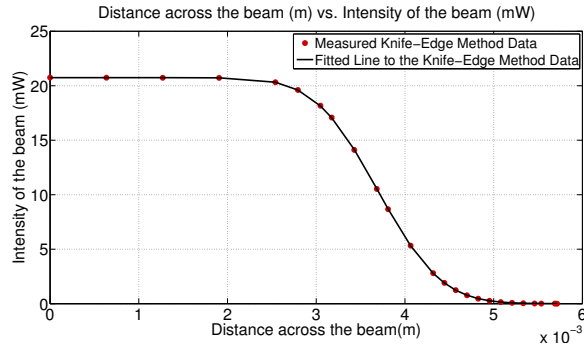


Figure 6: Measurement eleven

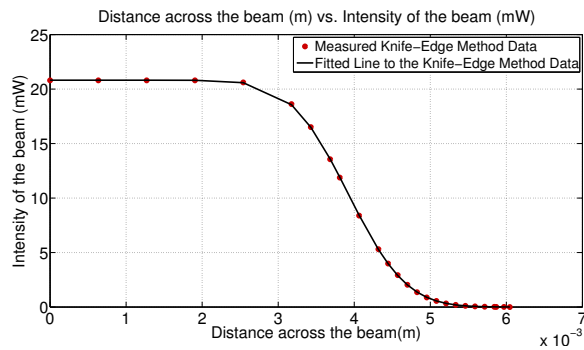


Figure 7: Measurement twelve

Figure 8: Graphical comparison of our measurements after they were fitted to the Gaussian error function.

From eq. 1, a MATLAB model was developed for reconstructing the beam profile from the values of the estimated beam radius as a function of  $z$ , which were obtained from fitting the twelve sets of knife-edge measurements to the Gaussian error function. The model is shown below:

$$w(z) = P(1) \sqrt{\left(1 + \left(\frac{\lambda(z - P(2))}{\pi P(1)^2}\right)^2\right)} \quad (10)$$

Where  $P(1) = w_0$  and  $P(2) = z_0$ .

The results obtained from fitting the knife-edge measurements to the Gaussian error function were then fitted to this new model, giving the final reconstructed beam profile shown in Fig. 10.

The beam parameters which were obtained using the knife-edge method are :  $w_0 = 200\mu m$  and  $z_0 = 0.0312m$ , where the origin of  $z$  is at the output of the laser head.

### 3.2.2 The Beam Profiler Measurement Method

The second method used to profile the Gaussian beam and obtain the beam parameters was through the use of a beam profiler. The optical setup was constructed, and then the laser was shone into a beam profiling camera, and the full waist at  $\frac{1}{e^2}$  of the irradiance distribution was recorded. These measurements were taken at various positions along the  $z$  axis, since the Gaussian beam propagates along the  $z$  axis, as stated earlier. They are shown in Table 3, and were fitted using the MATLAB model for reconstructing the beam profile that is described previously in Eq. 10.

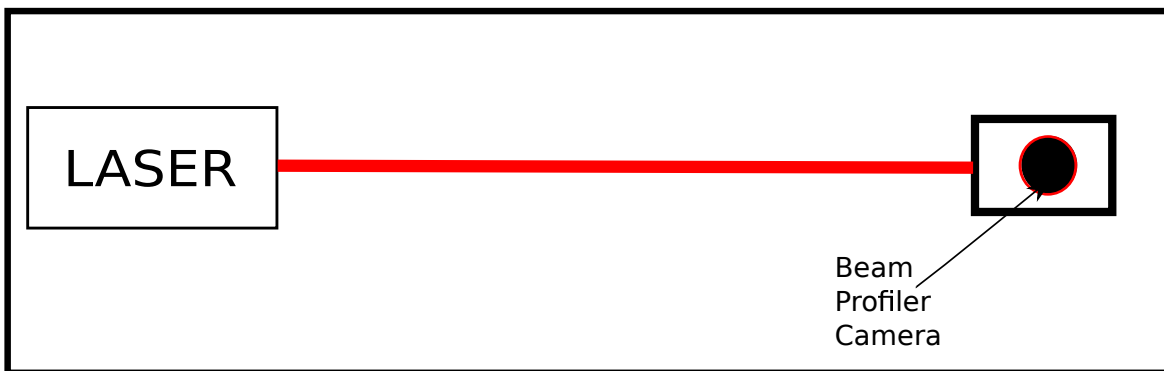


**Figure 9:** A diagram showing a simplified schematic of the setup for the beam profiler method.

The beam parameters which were obtained through the use of the beam profiler are :  $w_0 = 200\mu m$  and  $z_0 = -0.0133m$ .

The reconstructed beam profile obtained through the measurements taken with the beam profiler is shown in Fig. 10.

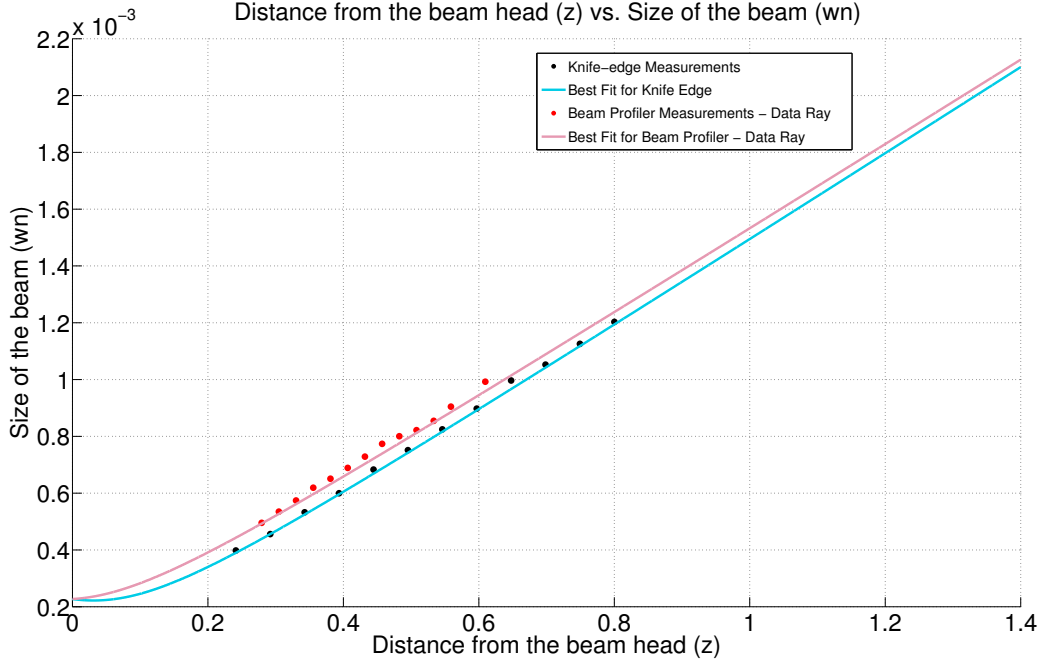


**Figure 10:** Graphical results showing a comparison of the constructed beam profiles from the measurements taken through the knife-edge technique and through using the beam profiler.

For both of the beam profiling methods, we obtained the same value for the waist of the beam, where  $w_0 = 200\mu\text{m}$ , however, we obtained differing values for the position of the waist. Because of this, we will take the average of these two values, and have a final waist value of  $z_0 = 0.009\text{m} \pm 0.022$ . Therefore, the final beam parameters which we will use for designing the mode matching telescope will be where  $w_0 = 200\mu\text{m}$  and  $z_0 = 0.009\text{m} \pm 0.022$ .

### 3.3 Mode Matching and a Beam Steering System

The mode matching of a Gaussian Beam involves the modification of the beam with multiple lenses. Essentially, the power in the beam is coupled to a specific beam waist radius and radius of curvature. When attempting to mode match a Gaussian Beam, the ABCD matrix law is applied to an already aligned optical setup. Then, the relations between the sizes and positions of the beam waists before and after the optical setup can be found and the correct beam waist radius and radius of curvature can be calculated. The mode matching and beam steering system will be integral in the construction and alignment for the mode matching telescope.

For our optical setup, we obtained the following beam parameters for our Gaussian beam with, the waist,  $w_0 = 200\mu\text{m}$ , and the position of the waist,  $z_0 = 0.009\text{m} \pm 0.022$ . We needed to incorporate optical components, such as a polarizing beam splitter, beam dumps, and a  $\frac{\lambda}{4}$  wave-plate, before incorporating our lens and mirrors into the setup. The polarizing beam splitter is a crucial part

of most interferometers, and separates the S and P polarization components by reflecting the S component at the dielectric beam splitter coating, while allowing the P component to pass. The beam dumps absorb any beams of light which go into them, and are typically a way of managing and reducing the back reflections and scattering of beams. Finally, the  $\frac{\lambda}{4}$  wave-plate is an optical device which affects the polarization state of the beam passing through it, and works through shifting the phase between two perpendicular polarization components of the beam.

For the optical setup, we needed two converging lens and four mirrors (the former two being used to fold the beam, and the latter being used to align the beam into the Michelson Interferometer). These components needed to be placed in such a way, that our end beam waist was approximately at  $z = 2m$  and  $w_0 = 300\mu m$ . We needed our final waist at a distance of  $2m$  away from the last lens, as a distance of approximately  $1.308m$  was needed from the point of entry of the beam into the vacuum chamber until the end mirrors. Also, the distance for the alignment mirrors and the initial optical components had to be taken into consideration. These constraints resulted in the final waist being at a distance of  $2m$ .

An additional constraint in the setup, is that the breadboard available has dimensions of  $18'' \times 18''$ ; the folding of the beam was necessary to accommodate this constraint. Also, the lenses which are being chosen for the mode matching telescope will only be from the following list of lenses, which are the ones available in the lab (the values given here are the focal lengths of the lenses) :  $250mm$ ,  $64.4mm$ ,  $254mm$ ,  $355.9mm$ ,  $40mm$ ,  $40.7mm$ ,  $406.6mm$ ,  $406mm$ ,  $100mm$ ,  $152.6mm$ ,  $500mm$ ,  $130mm$ ,  $400mm$ .

Several programming tools were used for the mode matching of the beam and as a rough design of the mode matching telescope, one of which was the “Jammt” software [4].

Fig. 11 was made using the “Jammt” software, and it gives a rough estimate as to where the main optical components should be positioned:

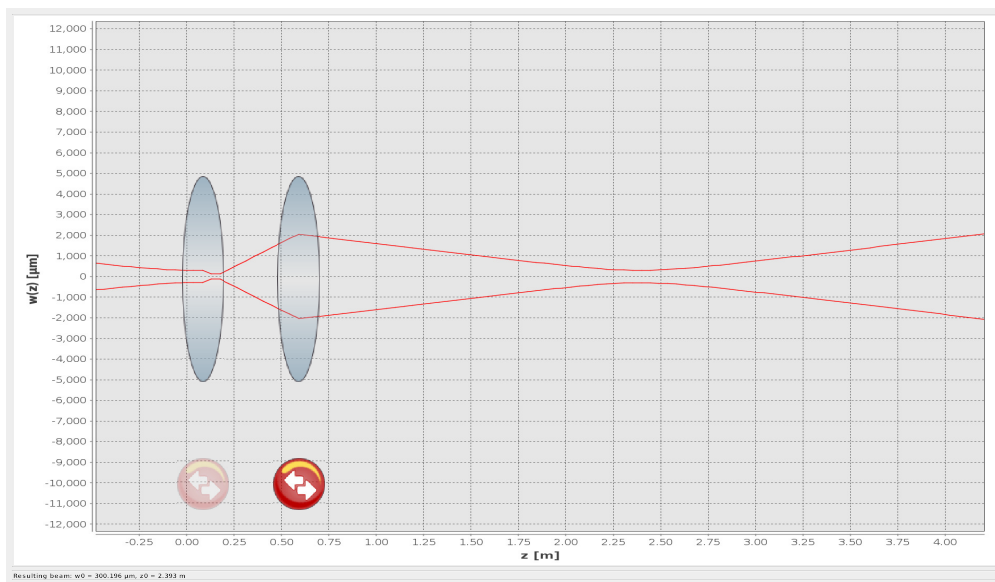


**Figure 11:** One of the designs for the mode matching telescope using the “Jammt” software.

Where the initial waist has the values of  $w_0 = 200\mu\text{m}$  and  $z_0 = 0.011\text{m} \pm 0.001$ , the first lens has a focal length of  $50.0\text{mm}$  and a position at  $0.086\text{m}$  from  $w_0$ , the second lens has a focal length of  $120.0\text{mm}$  and a position at  $0.591\text{m}$  from  $w_0$ , and the final waist has the values of  $w_0 = 300.0\mu\text{m}$  and  $z_0 = 3.253\text{m}$ .

### 3.4 Construction and Alignment of the Mode Matching Telescope

For our first design of the mode matching telescope, we chose the initial lens to have a focal length of  $80.0\text{mm}$  and our second lens to have a focal length of  $355.9\text{mm}$ . However, during our initial setup of the mode matching telescope, we realised that the lenses did not have the correct focal lengths, and thus we were forced to re-measure all of the focal lengths of the lenses. We obtained values which were vastly different to those which we made our initial schematics with, so we also had to redesign our mode matching telescope with the newly measured values.

We should note that the initial values of the two lens were chosen from a set of lens that were available in the lab (and whose focal points were re-measured). We chose the  $50.0\text{mm}$  lens to be the first lens since we required our beam to diverge quite strongly after it exited the laser head. To compensate for not having a concave lens which would have caused this strong divergence, we used a convex lens with a very small focal length which produced the strong divergence desired. The second lens was chosen to be  $120.0\text{mm}$ , as we needed a lens with a fairly average focal length.

Following this, we calculated the tolerances of the lenses for the optical system of the telescope. When we talk about measuring the "tolerances" of the lenses for our optical system, we are referring to what the dependence of the beam waist parameters in response to varying the position of our lenses. For our system, we needed the tolerance of our lenses to be such that slight movements of either of the lenses would not drastically change the size and position of the beam waist. In an ideal optical system, we would like some degree of freedom when varying the position of both of the lenses.

From the graph shown in [12](#), we found that there was a high dependence on the accuracy of the placement of the first lens, which affected both the size and position of the waist (more so than the second lens). The second lens was mostly used as the final alignment tool, as it mainly affected the position of the waist, although it did affect the size of the waist to a small extent as well.

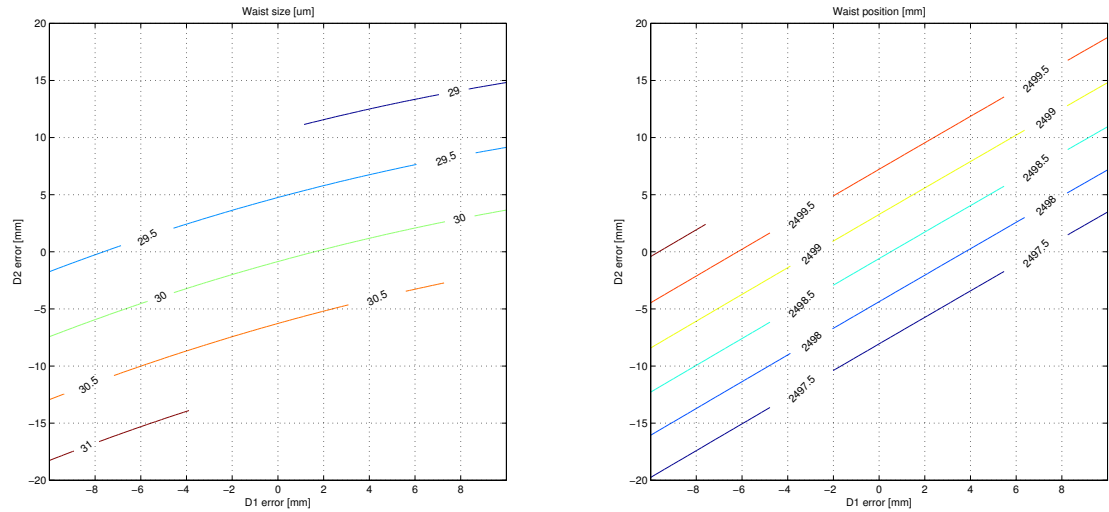


**Figure 12:** A graph showing the tolerances for Lens (1) and Lens (2).

Our final design for the mode matching telescope was constructed taking these lens tolerances into consideration in the alignment process, and the final schematic of the optical setup for the input telescope can be seen in [13](#).

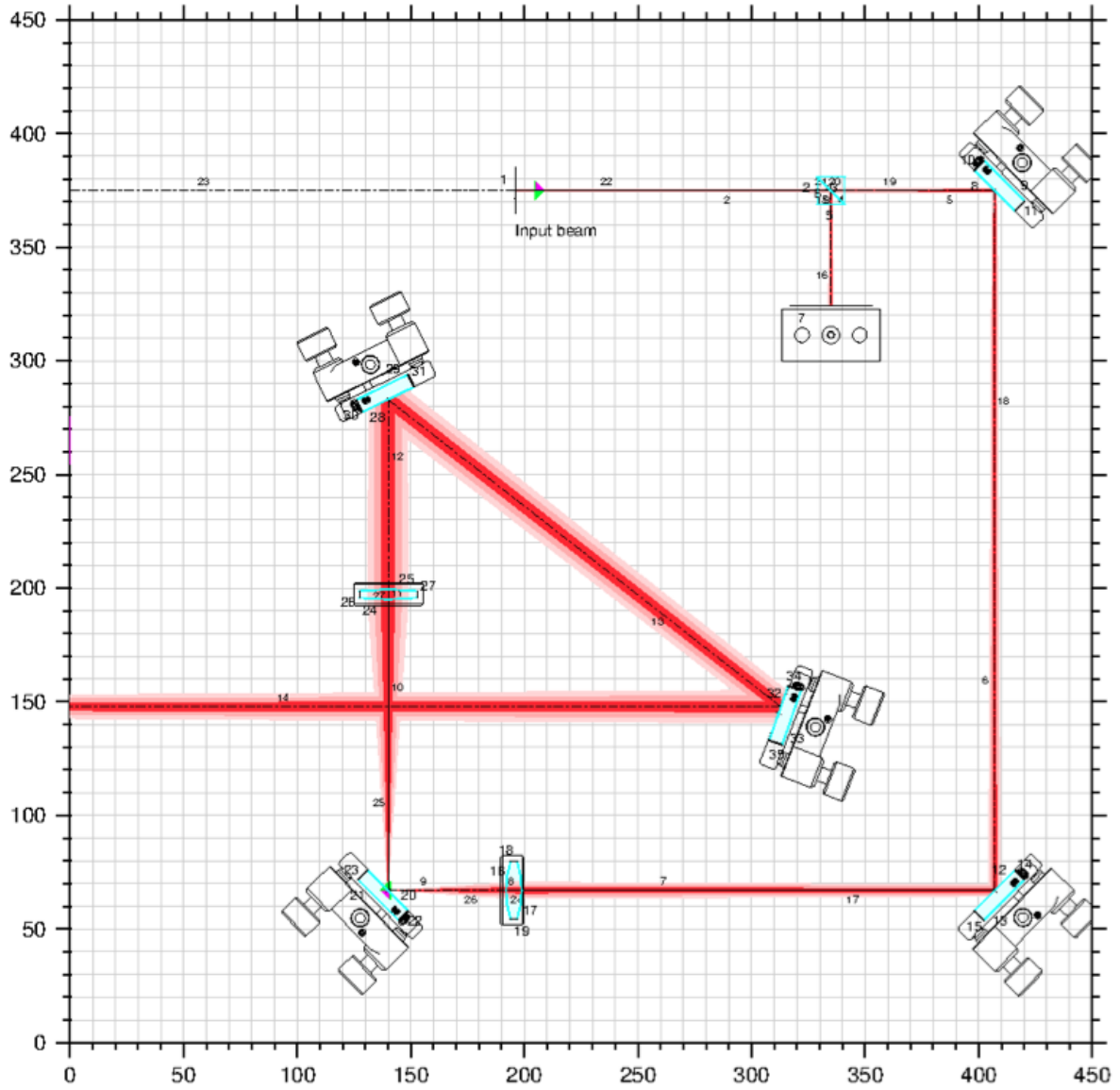


**Figure 13:** Detailed schematic diagram of the optical layout for the input telescope

### 3.5 Conclusion

We had a goal of creating a mode-matching telescope that would mode-match our laser beam to a waist of  $300\mu\text{m}$  at a distance of  $3.253\text{m}$  from the laser head. We managed to mode-match our laser beam to a waist of  $305\mu\text{m}$  at a distance of  $3.243\text{m}$  from the laser head.

### References

- [1] James P. Sethna, Karin A. Dahmen, Christopher R. Myers, “Crackling noise”, Nature 410, 242-250 (2001)
- [2] E. Quintero, E. Gustafson, R. Adhikari, “Experiment to investigate crackling noise in maraging steel blade springs”, LIGO-1300465-v2 (2013)
- [3] Xiaoyue Ni, Eric Quintero, Gabriele Vajente, “Proposal for an upgrade of the Crackle experiment”, LIGO-T1400407-v1 (2013)
- [4] N. Lastzka, A. Thring, “Jammt Software”, available at <http://www.sr.bham.ac.uk/dokuwiki/doku.php?id=geosim:jammt>.
- [5] Nicolas Smith, “A la mode MATLAB Toolbox”, available at <http://www.ligo.mit.edu/~nsmith/alm/almdemo.html#4>



**Table 1:** Results From Profiling the Beam Using the Knife-Edge Method [Measurement Three].

Distance across the beam (m)	Intensity of the beam (mW)
0	20.4000
0.001270	20.2800
0.002540	20.2200
0.003175	19.5200
0.003020	19.5200
0.003429	15.6800
0.003556	11.9900
0.003683	7.77000
0.003810	4.20000
0.003937	1.90000
0.004064	0.72000
0.004191	0.26000
0.004318	0.13000
0.004445	0.10000
0.004572	0.09000
0.004699	0.08000
0.004826	0.07000
0.004953	0.06000
0.005080	0.05000
0.005207	0.04000
0.005334	0.04000
0.005461	0.03000
0.005588	0.02000
0.005715	0.02000
0.005842	0.02000
0.005969	0.01000
0.006096	0.01000
0.006223	0.00000

**Table 2:** Results From Profiling the Beam Using the Knife-Edge [Method Measurement Eight].

Distance across the beam (m)	Intensity of the beam (mW)
0	21.0000
0.0006	20.9800
0.0013	20.8800
0.0019	18.3600
0.0020	16.9100
0.0022	14.9900
0.0023	12.8600
0.0024	10.5200
0.0025	8.2100
0.0027	6.0600
0.0028	4.2000
0.0029	2.7500
0.0030	1.6600
0.0032	0.9400
0.0033	0.5000
0.0034	0.2500
0.0036	0.1200
0.0037	0.0600
0.0037	0.0500
0.0037	0.0400
0.0038	0.0300
0.0038	0.0200
0.0039	0.0100
0.0040	0.0100
0.0041	0.0000

**Table 3:** Results From Profiling the Gaussian Beam Using the Beam Profiler.

Distance from the beam head (m)	Diameter of the beam (m)	Size of the Beam ( $m^{-4}$ )
0.2794	0.0009	4.95
0.3048	0.0011	5.34
0.3302	0.0011	5.74
0.3556	0.0012	6.19
0.3810	0.0013	6.51
0.4064	0.0014	6.89
0.4318	0.0015	7.29
0.4572	0.0015	7.74
0.4826	0.0016	8.00
0.5080	0.0016	8.21
0.5334	0.0017	8.54
0.5588	0.0018	9.05
0.6096	0.0020	9.92